A study of the excited electronic states of normal and fully deuterated furan by photoabsorption spectroscopy and high-level ab initio calculations

ARTICLE *in* JOURNAL OF MOLECULAR SPECTROSCOPY · MARCH 2015

Impact Factor: 1.48 · DOI: 10.1016/j.jms.2015.03.002

10 AUTHORS, INCLUDING:

Elaine Ann Seddon

The University of Manchester

122 PUBLICATIONS **1,144** CITATIONS

SEE PROFILE

Evgeniy V Gromov

Universität Heidelberg

32 PUBLICATIONS **603** CITATIONS

SEE PROFILE

Tatiana Korona

University of Warsaw

66 PUBLICATIONS **1,528** CITATIONS

SEE PROFILE

Journal of Molecular Spectroscopy xxx (2015) xxx–xxx

Contents lists available at ScienceDirect

Journal of Molecular Spectroscopy

journal homepage: www.elsevier.com/locate/jms

A study of the excited electronic states of normal and fully deuterated furan by photoabsorption spectroscopy and high-level ab initio calculations

D.M.P. Holland [a,*], E.A. Seddon [a], A.B. Trofimov [b,c], E.V. Gromov [b,d], M. Wormit [e], A. Dreuw [e], T. Korona [f], N. de Oliveira [g], L.E. Archer [g], D. Joyeux [g]

[a] Daresbury Laboratory, Daresbury, Warrington, Cheshire WA4 4AD, UK
[b] Laboratory of Quantum Chemistry, Irkutsk State University, 664003 Irkutsk, Russia
[c] Favorsky Institute of Chemistry, SB RAS, 664033 Irkutsk, Russia
[d] Theoretische Chemie, Physikalisch-Chemisches Institut, Universität Heidelberg, Im Neuenheimer Feld 229, D-69120 Heidelberg, Germany
[e] Interdisciplinary Centre for Scientific Computation, Universität Heidelberg, Im Neuenheimer Feld 368, D-69120 Heidelberg, Germany
[f] Faculty of Chemistry, University of Warsaw, ul. Pasteura 1, PL-02-093 Warsaw, Poland
[g] Synchrotron Soleil, Orme des Merisiers, St Aubin BP48, 91192 GIF sur Yvette Cedex, France

ARTICLE INFO

Article history:
Received 12 January 2015
In revised form 27 February 2015
Available online xxxx

Keywords:
Photoabsorption
Synchrotron radiation
Rydberg states
Ab initio excitation energies
Vibrational progressions

ABSTRACT

The photoabsorption spectra of C_4H_4O and C_4D_4O have been measured between ~5.5 and 17.7 eV using a synchrotron radiation-based Fourier transform spectrometer. In addition to several broad bands due to transitions into valence states, the spectra exhibit numerous sharp bands associated with Rydberg states belonging to series converging onto the $\tilde{X}\,^2A_2$ or the $\tilde{A}\,^2B_1$ state limits. Vertical excitation energies and oscillator strengths have been computed using the second- and third-order algebraic-diagrammic construction polarisation propagator methods (ADC(2) and ADC(3)), and the equation-of-motion coupled-cluster method at the level of singles and doubles model (EOM-CCSD). Adiabatic excitation energies have been estimated using previously computed corrections. The theoretical predictions have allowed assignments to be proposed for the Rydberg series observed in the present single-photon absorption spectra and for some additional series, mainly of A_2 symmetry, reported in previous multiphoton excitation studies. The assignments of some of the Rydberg series converging onto the $\tilde{A}\,^2B_1$ state limit have been revised and, guided by our calculations, the principal series is ascribed to the $2b_1 \rightarrow nda_2\ ^1B_2$ and $2b_1 \rightarrow ndb_1\ ^1A_1$ transitions. f-type Rydberg series, previously observed only in the multiphoton absorption spectrum of furan, have been observed and assigned. Such f-type series, converging onto either the $\tilde{X}^2A_2$ or the $\tilde{A}\,^2B_1$ state thresholds, contribute significantly to the single-photon absorption spectrum. Many of the absorption bands associated with Rydberg states display vibrational progressions which resemble those in the corresponding photoelectron band. It appears that some of the structure associated with the $1a_2 \rightarrow 3pb_2\ ^1B_1$ and $1a_2 \rightarrow 3pb_1\ ^1B_2$ transitions involves excitation of non-totally symmetric vibrational modes.

1. Introduction

The first few excited states of furan (Fig. 1) have attracted considerable attention due to their unusual and complex spectroscopic and dynamical properties. Extensive theoretical investigations have shown that the potential energy surfaces corresponding to the two lowest Rydberg states and to the two lowest valence excited states are vibronically coupled, and that the associated conical intersections affect both the photoabsorption spectrum [1–3] and the photochemical transformations [4–8]. The UV single-photon absorption spectrum of furan is well established [9–16], and is dominated by two very broad and intense bands, associated with valence states, centred at ~6 and 8 eV. Weak and irregular vibrational structure appears in the near-threshold region of the lower of these bands, and some much sharper and stronger peaks, due to Rydberg states belonging to series converging onto the ground ($\tilde{X}\,^2A_2$) state ionisation limit, have long been known in the higher energy region. However, a consistent set of assignments for the Rydberg structure has yet to be achieved.

* Corresponding author.
E-mail address: david.holland@stfc.ac.uk (D.M.P. Holland).

http://dx.doi.org/10.1016/j.jms.2015.03.002
0022-2852/

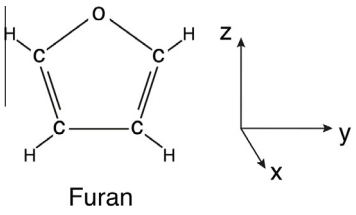

Fig. 1. Schematic representation of furan showing the axis orientation.

Recent progress towards an improved understanding of the Rydberg series converging onto the $\tilde{X}\,^2A_2$ state limit has been made in the mass-resolved (2 + 1) and (3 + 1) resonance enhanced multiphoton ionisation (REMPI) experiments on jet cooled C_4H_4O and C_4D_4O performed by Ridley et al. [17,18]. By taking advantage of the propensity rules which govern the relative intensities of two- or three-photon transitions, and by studying the polarisation dependence of the signal when using linearly or circularly polarised light, Ridley et al. were able to identify several d-type and f-type Rydberg series. Moreover, as the selection rules for two- or three-photon transitions differ from those for one-photon transitions, excited states of A_2 symmetry, which are forbidden in single-photon absorption from an initial state of A_1 symmetry, could be accessed. These studies were, nevertheless, hampered by the lack of theoretical predictions to guide the Rydberg state assignments.

An interesting point to emerge from the REMPI experiments [17,18] was the observation of structure attributed to *n*f Rydberg series. f-type Rydberg states have also been identified in recent high resolution photoabsorption studies of propyne [19] and 1-butyne [20], and their appearance has been discussed in relation to the character of the highest occupied molecular orbital (HOMO). In small molecules, the transition moment between the HOMO, which tends to be penetrating, and a Rydberg orbital of high orbital angular momentum (l), which tends to be non-penetrating, is small. However, in larger molecules the transition probability to such states may increase because the more extended nature of the molecular frame results in some of the high-l states having a penetrating character. The HOMOs in propyne and 1-butyne are similar [19–22], with both containing substantial atomic *n*p and *n*d character. As the single-photon selection rule for atomic transitions suggests that the oscillator strength for $l \rightarrow l+1$ transitions should be substantially higher than that for $l \rightarrow l-1$ transitions [23], the d-component of the HOMO should favour excitation into f-type Rydberg states. The HOMO in furan [22] has a nodal structure which resembles a distorted dπ orbital. Thus, in a simple, highly qualitative picture, the appearance of f-type Rydberg states in furan might not be unexpected.

In the present work, high resolution photoabsorption spectra of C_4H_4O and C_4D_4O have been recorded with the Fourier transform spectrometer (FTS) [24] at the Soleil synchrotron radiation facility. The photon energy range (5.5–17.7 eV) has allowed Rydberg series converging onto the $\tilde{X}\,^2A_2$, $\tilde{A}\,^2B_1$ or $\tilde{G}\,^2A_1$ state ionisation thresholds to be studied. The assignments of the observed structure are based on transition energies and oscillator strengths calculated in our complementary theoretical investigations.

The electronic excitation spectrum of furan has been the subject of many previous theoretical studies [15,25–33], the most relevant of which are those of Pastore et al. [32] using multireference perturbation theory (NEVPT), Wan et al. [30] employing the symmetry-adapted cluster configuration-interaction (SAC-CI) method, and Christiansen and Jørgensen [29] who performed linear response (LR) coupled cluster (CC) calculations using the CCSD and CC3 models. In this latter work, adiabatic transition energies were evaluated using excited-state geometry optimisation at the level of the CC2 model. Adiabatic energy corrections for many of the singlet excited states were also obtained in our previous ADC(2) study [28] where, for the first time, an attempt was made to interpret the experimental photoabsorption spectrum at a level beyond the vertical excitation picture.

To facilitate the assignment of the structure observed in the present photoabsorption spectrum, transition energies and oscillator strengths of the vertical excitations have been computed using the ADC(3) [34–36], ADC(2) [37–41] and (EOM-CCSD) [42–45] approaches. An extended basis set, which included f-type Rydberg functions, has been employed in these calculations, thereby allowing many of the Rydberg states to be reproduced. The inclusion of f-type Rydberg functions proved to be an important step because some of the most intense bands in the experimental spectrum are due to such excitations. Adiabatic excitation energies have been estimated using corrections computed at the ADC(2) level in earlier work [28]. Since the CCSD results are generally only slightly less accurate than the ADC(3) results [34,35], we use both sets of data to check the consistency of our predictions. For the same reason, we compare our results with those of Christiansen and Jørgensen [29], which are the best, already available, theoretical estimates.

2. Experimental apparatus and procedure

The photoabsorption spectra of C_4H_4O and C_4D_4O were recorded using the FTS [24] attached to the DESIRS beamline [46] at the Soleil synchrotron radiation source. Detailed descriptions of the beamline, spectrometer and experimental procedure have been reported in our previous work on thiophene [47] so only a brief account is given here.

The undulator-based beamline provides radiation covering the energy range ~5–40 eV, and a portion of this distribution, with a bandwidth of ~7% of the central energy, can be selected by tuning the undulator. This radiation passes through a cell containing the gaseous sample before entering the FTS. Two types of cell were used in the present work. The first was windowless and, by employing long entrance and exit capillaries, maintained a quasi-static column of gas, thereby allowing a relative absorption spectrum to be measured across the entire photon energy range. The second cell used MgF_2 entrance and exit windows, and was used to determine the absolute photoabsorption cross section over a limited energy range. The latter spectrum was used to calibrate the full VUV spectrum obtained with the windowless cell, with the resulting experimental uncertainty being about ±10%. This estimation represents an upper limit of the potential error at the high photon energy end of the spectrum. It is difficult to provide a more precise evaluation due to the complicated nature of assembling a composite spectrum from the individual sections. A detailed discussion of this process, together with a consideration of the energy dependent sources of error, will be given in a forthcoming publication [48].

The photon energy scale, which is intrinsically linear, was calibrated by using the absorption line due to the Ar $3p^6\ ^1S_0 \rightarrow 3p^5(^2P_{1/2})4s$ transition at 11.8282 eV [49]. A small peak due to this state appears in the absorption spectrum and originates from the gas filter used to attenuate the high harmonics.

The composite photoabsorption spectra of C_4H_4O and C_4D_4O, plotted in Fig. 2, have been assembled by combining those measured in the individual, overlapping spectral windows (undulator settings). The spectra shown were recorded with resolutions of 0.86 and 1.07 meV (FWHM) for C_4H_4O and C_4D_4O, respectively. Spectra measured with a resolution of 0.43 meV revealed no additional features. Thus, the line widths of the absorption bands are not resolution limited. The absolute photoabsorption cross

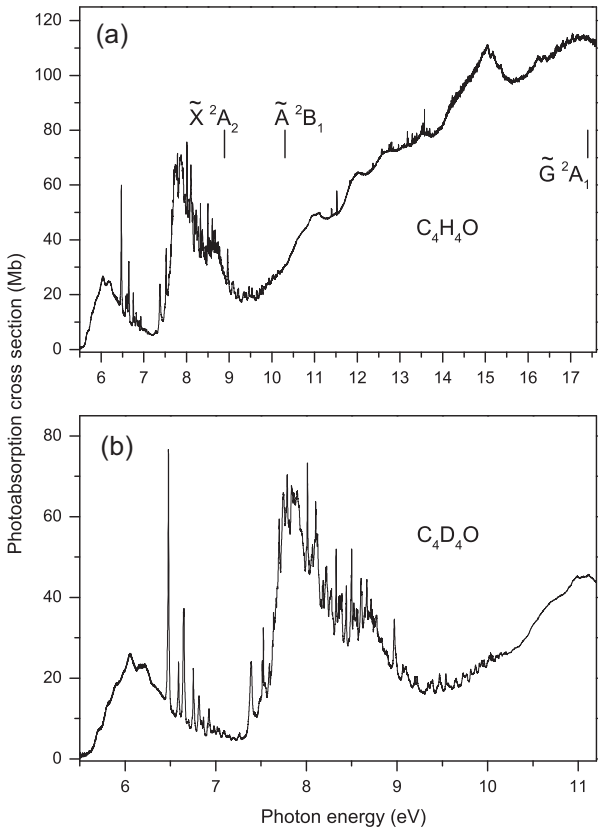

Fig. 2. The photoabsorption spectra of C_4H_4O (a) and C_4D_4O (b). The $\tilde{X}\ ^2A_2$, $\tilde{A}\ ^2B_1$ and $\tilde{G}\ ^2A_1$ state ionisation thresholds are marked. The sharp absorption lines occurring in the excitation range ~11–14 eV in C_4H_4O are due to atomic and molecular impurities. Most of these impurity lines can be attributed to CO, which is produced from the photolysis of furan by the synchrotron radiation.

sections, in regions devoid of sharp features, are in good agreement with those obtained previously by Rennie et al. [16]. However, the peak intensity in narrow absorption bands is greater in the present study due to the improved resolution.

Most of the bands appearing in the absorption spectrum belong to Rydberg series. For an unperturbed Rydberg state, the transition energy is given by

$$E_{n^*} = E_\infty - \frac{R}{n^{*2}}$$

where E_∞ is the relevant ionisation energy, R is the Rydberg constant (109736.44 and 109736.49 cm^{-1} for C_4H_4O and C_4D_4O, respectively) and n^* is the effective principal quantum number, $n^* = n - \delta_l$ where δ_l is the quantum defect for the l series. Previous studies have established that, for a particular value of l, δ_l generally lies within a small range and is almost independent of n for an unperturbed series. For ns, np, nd and nf series, δ_l is expected to have values which lie in the ranges (0.8–1.0), (0.4–0.7), (-0.2–0.2) and (-0.2–0.2), respectively. In our analysis of the experimental spectrum and the evaluation of the quantum defects, we have used adiabatic ionisation energies of 8.8863 [17], 10.308 [49] and 17.4 eV [49], for the $(1a_2)^{-1}$ $\tilde{X}\ ^2A_2$, $(2b_1)^{-1}$ $\tilde{A}\ ^2B_1$ and $(7a_1)^{-1}$ $\tilde{G}\ ^2A_1$ states, respectively.

Many of the Rydberg states observed in the photoabsorption spectrum exhibit accompanying vibrational structure. Since the molecular geometry of a Rydberg state is generally similar to that of the ionic state onto which the series converges, the Franck–Condon factor connecting the ground and Rydberg state is expected to be similar to that connecting the ground and corresponding ionic state. Therefore the vibrational structure appearing in the photoabsorption spectrum has been assigned through comparison with that in the associated photoelectron band. HeI excited photoelectron spectra of C_4H_4O [16,50,51] and C_4D_4O [16] have been reported previously, and the zero kinetic energy (ZEKE) photoelectron spectrum of C_4H_4O has also been measured [52].

3. Computational details

The ADC(3) polarisation propagator approach [34,35], which has recently been implemented efficiently [36] into the Q-Chem program [53] was employed to compute the vertical electronic excitation energies of furan. The ADC(3) method treats excited electronic states, dominated by singly excited configurations, through third-order in perturbation theory and requires computational effort that scales as N^6 with respect to the number of molecular orbitals N. A comparable theoretical description of excited states is achieved only in the well-known CC3 model, although this model requires a larger computational effort, which scales as N^7. The latter constraint makes CC3 computations impractical in situations where an extended basis set and many roots of the secular equations are required. In furan, the UV photoabsorption spectrum is dominated by singly excited Rydberg states and only a few valence-type excited states show an increased contribution from double excitations. Therefore, in this case, the improved treatment of states with double excitation character, facilitated by the CC3 model, is not really necessary. Since the ADC(3) treatment of the dipole transition moment is not available, these quantities were computed at the ADC(2) level [37–40], yielding the so-called ADC(3/2) approximation scheme for the dipole oscillator strengths. The ADC(2) computations were performed using both the Q-Chem [39,41,53] and the MOLPRO [40,54,55] implementations at the so-called 'strict' level of approximation [37,38]. The EOM-CCSD [42–45] computations were carried out using the MOLPRO program [54,55]. In addition to the vertical excitation energies and oscillator strengths, these computations also provided the dipole moments and the second electronic moments of the final states. The equilibrium ground state geometrical parameters were taken from the experimental work of Mata et al. [56]. The basis set was constructed from the aug-cc-pVTZ set [57,58] on atoms and from s, p, d and f-type Rydberg functions [59], each taken with effective quantum numbers n_e = 3, 3.5, 4, 4.5, 5, placed on the molecular centre of gravity. The total number of molecular orbitals in this basis was 402. A molecular symmetry of C_{2v} was adopted in the EOM-CCSD and ADC Q-Chem calculations. Adiabatic corrections, taken from our previous ADC(2) study [28] and from the work of Christiansen and Jørgensen [29], were added to the vertical excitation energies to obtain estimates of the adiabatic transition energies. The former set of corrections was obtained using the linear vibronic coupling (LVC) approach [60], whereas the latter set resulted from the explicit excited-state geometry optimisation at the level of the CC2 model. The EOM-CCSD and the ADC(2) results obtained here for the vertical and adiabatic transitions of furan are directly comparable with our previous computations on thiophene [47].

4. Preliminary considerations and review of theoretical results

According to our computations, the ground state Hartree–Fock electronic configuration of furan may be written as

Core: $(1a_1)^2\ (1b_2)^2\ (2a_1)^2\ (3a_1)^2\ (2b_2)^2$
Valence shell: $(4a_1)^2\ (5a_1)^2\ (3b_2)^2\ (4b_2)^2\ (6a_1)^2\ (7a_1)^1\ (1b_1(\pi_1))^2$ $(5b_2)^2\ (6b_2)^2\ (8a_1)^2\ (9a_1)^2\ (2b_1(\pi_2))^2\ (1a_2(\pi_3))^2\ \tilde{X}\ ^1A_1$

where the orbitals are numbered using C_{2v} point group symmetry (Fig. 1). The π-orbital manifold forming the conjugate system comprises three occupied orbitals (namely, the $1a_2(\pi_3)$ (HOMO) and the $2b_1(\pi_2)$ (HOMO-1), as well as the more tightly bound $1b_1(\pi_1)$) and two low-lying unoccupied orbitals. These two vacant orbitals, which are conventionally labelled $3b_1(\pi_4^*)$ and $2a_2(\pi_5^*)$, are the antibonding counterparts of the $2b_1(\pi_2)$ and $1a_2(\pi_3)$ orbitals, respectively. The actual sequential numbers of the π_4^* and π_5^* orbitals, obtained from the ab initio calculations, may be different from those given, but we use this nomenclature for simplicity. Thus, these orbital numbers should be regarded as symbolic (corresponding to a minimal basis set model) and are not directly related to the calculations.

Electron promotion from either the π_2 or the π_3 orbital, into various vacant valence or Rydberg orbitals, gives rise to the majority of the structure observed in the UV absorption spectrum. Four valence excited singlet states are expected from the $\pi \rightarrow \pi^*$ transitions. Two of these states, of B_2 symmetry, arise from the $1a_2(\pi_3) \rightarrow 3b_1(\pi_4^*)$ and the $2b_1(\pi_2) \rightarrow 2a_2(\pi_5^*)$ transitions. The other two states, due to the $2b_1(\pi_2) \rightarrow 3b_1(\pi_4^*)$ A_1 and the $1a_2(\pi_3) \rightarrow 2a_2(\pi_5^*)$ A_1 transitions, mix to form an antisymmetric (A_1^-) and a symmetric (A_1^+) pair of states. The A_1^- state has the lower excitation energy and spectral intensity, and, according to our ab initio results, it is also characterised by a considerable double excitation content.

The present ADC(3) and EOM-CCSD excitation energies and oscillator strengths for the vertical and adiabatic transitions of furan are listed in Table 1. The table also contains adiabatic excitation energies obtained by adding the adiabatic corrections available from previous studies [28,29] to the present vertical excitation energies. The LR-CCSD/CC3 estimates [29] are given for comparison.

A more detailed compilation of the present ADC(3) and ADC(2) results, together with our previous ADC(2) computations, can be found in Table S1 in Supplementary Material. A comparison between the present ADC(3) and ADC(2) data shows that the improved treatment of electron correlation at the ADC(3) level generally slightly decreases the vertical excitation energies. The mean absolute deviation between the two schemes for the transitions compared in Table S1 is ~0.1 eV, with the maximum absolute deviation being 0.3 eV. The comparison between the present ADC(2) results and the data obtained in our previous computations [28], where a much smaller basis set was employed, shows that the improvement in the basis set increases the excitation energies by ~0.2–0.3 eV.

Tables S2–S4 in Supplementary Material show the complete list of our EOM-CCSD results for the $1a_2(\pi_3) \rightarrow nl\gamma$ and $2b_1(\pi_2) \rightarrow nl\gamma$ Rydberg transitions and for the valence-type transitions, respectively. These tables include the quantum defects for the vertical transitions, the dipole moments and the second electronic moments for the final states.

The proposed assignments for the calculated transitions to various Rydberg and valence-type states are, to a certain extent, approximate. In order to characterise the type of transition, we have taken into account symmetry considerations, as dictated by the electric-dipole selection rules, as well as the computed quantum defects, oscillator strengths and second electronic moments. The overall picture which emerges looks reasonably consistent. The calculated quantum defects are within the expected range and members of the same orbital multiplet lie fairly close in energy. As expected, the valence-type excited states, unlike the Rydberg states, are characterised by more compact electron density distributions. The corresponding transitions have considerable oscillator strengths and their excitation energies do not fit into Rydberg series. Valence states can perturb Rydberg states of the same symmetry. Thus, Rydberg–valence mixing, in certain cases, as well as Rydberg–Rydberg mixing at higher energies, cannot be excluded.

The present theoretical results provide, to the best of our knowledge, the most complete and accurate description of the furan absorption spectrum. As can be seen from Table 1, the ADC(3) and EOM-CCSD results are quite consistent with each other, with the mean difference between the vertical excitation energies being within the usual limits (~0.2 eV) of the error expected in these methods [35]. An even better agreement is achieved between the present ADC(3) vertical excitation energies and the CCSD/CC3 estimates [29]. In this case the mean deviation is 0.13 eV, and the maximal deviation, for the valence-type $1a_2(\pi_3) \rightarrow 2a_2(\pi_5^*)$ $^1A_1$ transition, is 0.25 eV. The present results are also consistent with those of other high-level computations, mentioned in the Introduction, and reviewed by Stenrup and Larson [7], for several of the lowest excited states (see Table 1 in [7]).

5. Results and discussion

5.1. Overview

Three bands, centred at ~6.0, 7.9 and 8.7 eV, dominate the photoabsorption spectrum of furan at energies below 10 eV (Fig. 2). The high intensity and broadness of these bands indicate that they contain significant contributions from excitations into valence states. The present calculations show, in accord with most previous theoretical results, that the lowest-lying band is due primarily to the $1a_2(\pi_3) \rightarrow 3b_1(\pi_4^*)$ $^1B_2$ transition. The next band, around 7.9 eV, arises mainly from the $1a_2(\pi_3) \rightarrow 2a_2(\pi_5^*)$ $^1A_1$ transition, although the upper state also has some Rydberg character. Another state of mixed valence-Rydberg character is predicted to be responsible for the peak at 8.7 eV.

Most of the narrow bands observed between ~6.4 and 10.2 eV can be attributed to Rydberg series converging onto either the $\tilde{X}\,^2A_2$ state limit at 8.8863 eV [17] or onto the $\tilde{A}\,^2B_1$ state limit at 10.308 eV [50]. In addition, some bands appearing between ~15 and 17.5 eV are associated with Rydberg series converging onto the $\tilde{G}\,^2A_1$ state limit at 17.4 eV [50].

In preparation for our discussion of Rydberg states involving transitions from either the $1a_2$ or the $2b_1$ orbital, we list the series to be considered. Single-photon excitation from the $1a_2$ orbital may give rise to the following series: npb_1 B_2, npb_2 B_1, nda_2 A_1, ndb_1 B_2, ndb_2 B_1, nfa_2 A_1, nfb_1 $B_2(2)$ and nfb_2 $B_1(2)$. Similarly, single-photon excitation from the $2b_1$ orbital may give rise to the following series: nsa_1 B_1, npa_1 B_1, npb_1 A_1, nda_1 $B_1(2)$, nda_2 B_2, ndb_1 A_1, nfa_1 $B_1(2)$, nfa_2 B_2 and nfb_1 $A_1(2)$. Single-photon selection rules forbid transitions into a final state of A_2 symmetry from an initial state of A_1 symmetry.

Ridley et al. [17] have determined the adiabatic ionisation energy of the $\tilde{X}\,^2A_2$ state in C_4H_4O and found it to be the same as that in C_4D_4O to within ±3 cm^{-1} (0.37 meV). As the Rydberg constants for the two isotopomers are almost identical, these conditions result in the absorption band due to an adiabatic transition into a Rydberg state in C_4H_4O appearing at almost the same excitation energy as does the corresponding band in C_4D_4O. Thus, a comparison between the photoabsorption spectra of the two isotopomers facilitates the identification of Rydberg state origins. It is noticeable that deuteration sharpens some of the Rydberg absorption bands.

For the most part, our discussion of the Rydberg states is carried out in relation to the structure in the photoabsorption spectrum of C_4H_4O. However, Figs. 3–6 show the spectra for both isotopomers, and the corresponding transition energies and assignments are listed in Tables 2–6.

Table 1
Energies Ω (eV) and oscillator strengths f (a.u.) of vertical (v) and adiabatic (0–0) electronic excitations in furan obtained in the present ADC(3) and EOM-CCSD computations and previous LR-CCSD/CC3[a] estimates.

Excitation		ADC(3) [b]				LR-CCSD/CC3 [a]			EOM-CCSD [b]		
		Ω_v	f_v	Ω_{0-0} [c]	Ω_{0-0} [d]	Ω_v	f_v	Ω_{0-0} [e]	Ω_v	f_v	Ω_{0-0} [c]
$^1A_2$	$1a_2 \rightarrow 3sa_1$	5.91		5.58	5.76	6.04		5.89	6.12		5.79
$^1B_2$	$1a_2 \rightarrow 3b_1(\pi_4^*)$	6.10	0.167	5.85	5.67	6.32	0.144	5.89	6.45	0.174	6.20
$^1B_1$	$1a_2 \rightarrow 3pb_2$	6.45	0.036	6.32	6.31	6.58	0.035	6.44	6.66	0.036	6.53
$^1A_2$	$1a_2 \rightarrow 3pa_1$	6.60		6.46	6.43	6.73		6.56	6.81		6.67
$^1A_1$	$2b_1 \rightarrow 3b_1(\pi_4^*)$	6.44	<0.001	6.11	6.00/5.87	6.57	<0.001	6.13/6.00	6.82	<0.001	6.49
$^1B_2$	$1a_2 \rightarrow 3pb_1$	6.72	0.001	6.56	6.56	6.86	0.015	6.70	6.94	<0.001	6.78
$^1A_2$	$1a_2 \rightarrow 3da_1$	6.91		6.81	6.74	7.05		6.88	7.13		7.03
$^1B_1$	$1a_2 \rightarrow 3db_2$	7.13	<0.001	7.10	6.98	7.26	0.001	7.11	7.34	<0.001	7.31
$^1A_2$	$1a_2 \rightarrow 3\bar{d}a_1$	7.17		7.06	7.00	7.33		7.16	7.38		7.27
$^1A_1$	$1a_2 \rightarrow 3da_2$	7.39	<0.001	7.24	7.24	7.53	<0.001	7.38	7.59	<0.001	7.44
$^1B_1$	$2b_1 \rightarrow 3sa_1$	7.49	0.031	7.46	7.40	7.46	0.022	7.37	7.54	0.024	7.51
$^1A_2$	$1a_2 \rightarrow 4sa_1$	7.52		7.42					7.71		7.61
$^1B_2$	$1a_2 \rightarrow 3db_1$	7.52	0.010	7.34	7.33	7.66	0.016	7.47	7.72	0.012	7.54
$^1B_1$	$1a_2 \rightarrow 4pb_2$	7.72	0.002	7.57					7.92	0.003	7.77
$^1A_2$	$1a_2 \rightarrow 4pa_1$	7.75		7.71					7.94		7.90
$^1B_2$	$1a_2 \rightarrow 4pb_1$	7.76	0.003	7.61					7.95	0.004	7.80
$^1A_2$	$1a_2 \rightarrow 4da_1$	7.85		7.71					8.04		7.90
$^1B_1$	$1a_2 \rightarrow 4db_2$	7.91	<0.001	7.80					8.10	<0.001	7.99
$^1A_2$	$1a_2 \rightarrow 4\bar{d}a_1$	7.91		7.76					8.10		7.95
$^1A_1$	$1a_2 \rightarrow 2a_2(\pi_5^*)$	7.88	0.237	7.78	7.52/7.04	8.13	0.350	7.77/7.29	8.12	0.120	8.02
$^1A_2$	$1a_2 \rightarrow 4fa_1$	7.93							8.13		
$^1B_1$	$1a_2 \rightarrow 4fb_2$	7.95	<0.001						8.12	0.001	
$^1B_1$	$1a_2 \rightarrow 4\bar{f}b_2$	7.98	0.006						8.17	0.004	
$^1B_2$	$1a_2 \rightarrow 4fb_1$	7.98	0.003						8.17	0.003	
$^1B_1$	$2b_1 \rightarrow 3pa_1$	8.13	0.002	8.01	8.14	8.07	0.002	<8.03	8.20	0.005	8.08
$^1A_2$	$2b_1 \rightarrow 3pb_2$	8.14		8.10		8.08		<8.04	8.17		8.13
$^1A_2$	$1a_2 \rightarrow 5sa_1$	8.01		7.84					8.20		8.03
$^1B_2$	$1a_2 \rightarrow 4\bar{f}b_1$	8.01	<0.001						8.20	<0.001	
$^1A_1$	$1a_2 \rightarrow 4da_2$	8.02	0.007	7.91					8.21	0.004	8.10
$^1A_2$	$1a_2 \rightarrow 4\bar{f}a_1$	8.07							8.28		
$^1B_2$	$1a_2 \rightarrow 4db_1$	8.08	0.003	7.91					8.27	0.003	8.10
$^1A_1$	$1a_2 \rightarrow ?a_2(\pi^*)/4fa_2$	8.08	0.125						8.37	0.178	
$^1B_1$	$1a_2 \rightarrow 5pb_2$	8.17	0.002	8.06					8.36	0.002	8.25
$^1B_2$	$1a_2 \rightarrow 5pb_1$	8.19	0.002	8.04					8.38	0.003	8.23
$^1A_2$	$1a_2 \rightarrow 5pa_1$	8.19		7.71					8.38		7.90
$^1A_1$	$2b_1 \rightarrow 3pb_1$	8.23	0.006	8.13		8.22	0.016	8.13	8.28	0.021	8.18
$^1A_2$	$1a_2 \rightarrow 5da_1$	8.23							8.42		
$^1B_1$	$1a_2 \rightarrow 5db_2$	8.25	<0.001						8.44	<0.001	
$^1A_2$	$1a_2 \rightarrow 5\bar{d}a_1$	8.26							8.45		
$^1A_2$	$1a_2 \rightarrow 5fa_1$	8.27							8.46		
$^1B_1$	$1a_2 \rightarrow 5fb_2$	8.29	0.003						8.48	0.005	
$^1B_1$	$1a_2 \rightarrow 5\bar{f}b_2$	8.30	0.004						8.49	0.004	
$^1B_2$	$1a_2 \rightarrow 5fb_1$	8.30	0.003						8.49	0.003	
$^1A_2$	$1a_2 \rightarrow 5\bar{f}a_1$	8.32							8.51		
$^1B_2$	$1a_2 \rightarrow 5\bar{f}b_1$	8.32	<0.001						8.51	<0.001	
$^1A_1$	$1a_2 \rightarrow 5da_2$	8.32	0.003						8.53	<0.001	
$^1B_1$	$2b_1 \rightarrow 3da_1$								8.56	0.002	
$^1A_1$	$1a_2 \rightarrow 5fa_2$	8.34	0.012						8.57	0.080	
$^1B_2$	$1a_2 \rightarrow 5db_1$	8.36	0.001						8.55	0.002	
$^1B_2$	$1a_2/2b_1 \rightarrow ?$	8.86	0.085	8.69					8.88	0.040	8.71
$^1B_2$	$2b_1 \rightarrow 3da_2$								9.09	0.053	
$^1A_1$	$2b_1 \rightarrow 3db_1$	9.07	0.020						9.10	0.040	
$^1B_1$	$2b_1 \rightarrow 4sa_1$								9.11	0.002	
$^1B_1$	$9a_1 \rightarrow ?$								9.23	0.001	
$^1B_1$	$2b_1 \rightarrow 4pa_1$								9.33	0.003	
$^1A_1$	$2b_1 \rightarrow 4pb_1$	9.31	0.033						9.33	0.002	
$^1A_1$	$2b_1 \rightarrow 4fb_1$	9.33	0.013						9.57	0.001	
$^1A_1$	$2b_1 \rightarrow 4\bar{f}b_1$								9.59	<0.001	
$^1B_2$	$2b_1 \rightarrow 4fa_2$								9.60	0.004	
$^1B_2$	$2b_1 \rightarrow 4da_2$								9.64	0.002	
$^1A_1$	$2b_1 \rightarrow 4db_1$								9.65	0.008	
$^1A_1$	$2b_1 \rightarrow 5pb_1$								9.77	0.001	
$^1A_1$	$2b_1 \rightarrow 5fb_1$								9.89	0.001	
$^1A_1$	$2b_1 \rightarrow 5\bar{f}b_1$								9.90	<0.001	
$^1B_2$	$2b_1 \rightarrow 5fa_2$								9.90	0.002	

(*continued on next page*)

Table 1 (*continued*)

Excitation		ADC(3) [b]				LR-CCSD/CC3 [a]			EOM-CCSD [b]		
		Ω_v	f_v	Ω_{0-0} [c]	Ω_{0-0} [d]	Ω_v	f_v	Ω_{0-0} [e]	Ω_v	f_v	Ω_{0-0} [c]
$^1B_2$	$2b_1 \rightarrow 5da_2$								9.92	<0.001	
$^1A_1$	$2b_1 \rightarrow 5db_1$								9.93	0.003	

[a] LR-CCSD calculations using the cc-pVTZ basis set augmented by atom centred (spd/sp) and ring centred (7s7p7d) diffuse basis functions including correction due to triple excitations, estimated from the difference between the CC3 and CCSD energies using the ANO basis [29]. The oscillator strengths *f* are computed at the CCSD level.

[b] Present calculations using the aug-cc-pVTZ basis set augmented by ring centred (5s5p5d5f) diffuse basis functions. The oscillator strengths *f* are computed using the ADC(3/2) approximation scheme, see text for details.

[c] Adiabatic transition energies obtained using the presently calculated vertical excitation energies and our previous ADC(2) adiabatic corrections [28] (see Table S1 of Supplementary Material and text for details).

[d] Adiabatic transition energies obtained using the present ADC(3) vertical transition energies and adiabatic corrections evaluated as LR-CC2 differences between vertical and adiabatic excitation energies for double-zeta (DZP and DZPR) basis sets [29]. In the case of the $^1A_1$ valence excited states, results for both symmetric C_{2v} and symmetry broken C_s energy minima are shown.

[e] Adiabatic transition energies obtained using the LR-CCSD/CC3 vertical transition energies [29] and adiabatic corrections described in footnote [d].

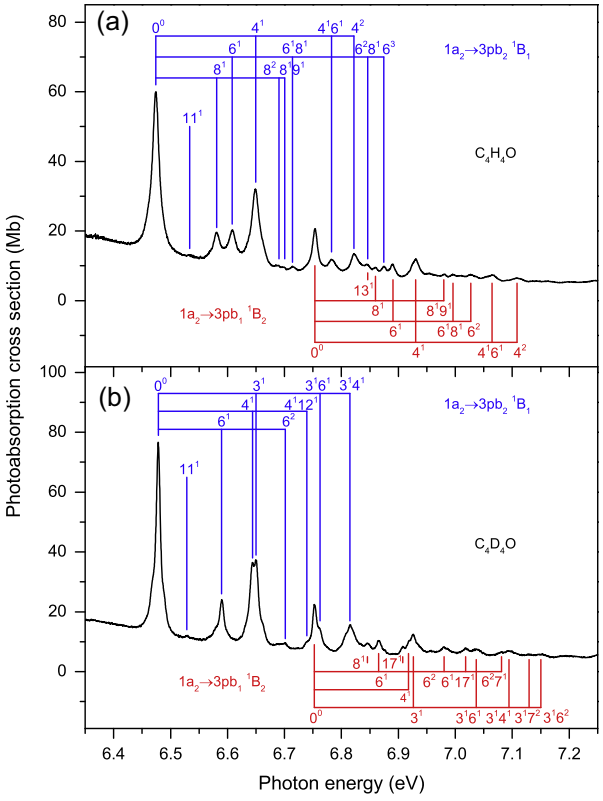

Fig. 3. The photoabsorption spectra of C_4H_4O (a) and C_4D_4O (b) showing structure due to the $1a_2 \rightarrow 3pb_2\ ^1B_1$ and $1a_2 \rightarrow 3pb_1\ ^1B_2$ Rydberg transitions. Excitation energies and assignments are given in Table 2.

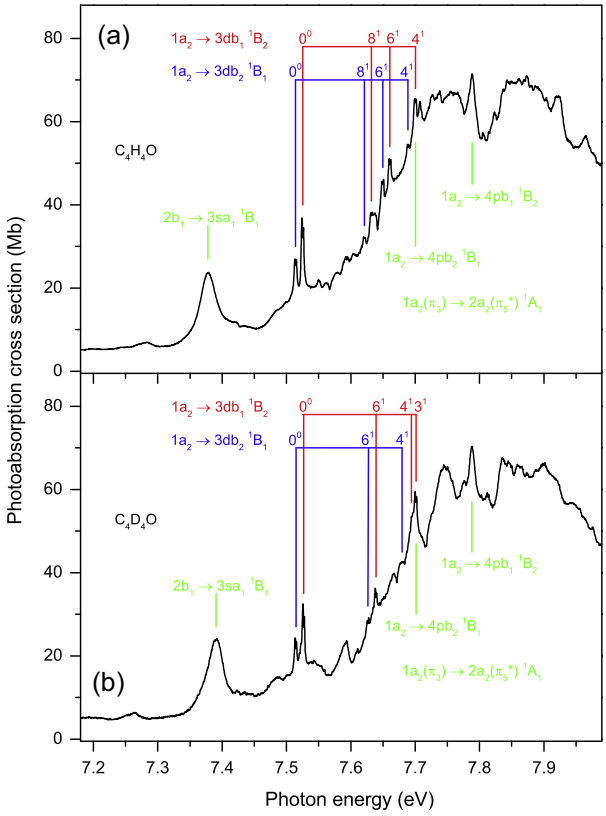

Fig. 4. The photoabsorption spectra of C_4H_4O (a) and C_4D_4O (b) showing structure due to the $1a_2(\pi_3) \rightarrow 2a_2(\pi_5^*)\ ^1A_1$ valence transition, and to the $1a_2 \rightarrow 3db_1\ ^1B_2$, $1a_2 \rightarrow 3db_2\ ^1B_1$, $1a_2 \rightarrow 4pb_2\ ^1B_1$, $1a_2 \rightarrow 4pb_1\ ^1B_2$ and $2b_1 \rightarrow 3sa_1\ ^1B_1$ Rydberg transitions. Excitation energies and assignments are given in Tables 3 and 4.

5.2. Valence states

The very broad band observed between ~5.5 and 7.0 eV, and the weak and irregular superimposed structure occurring between ~5.6 and 6.4 eV have been discussed in detail previously [1–3,15,26–32], and will only be considered briefly here. The present ADC(3) results (Table 1) predict that only the $1a_2(\pi_3) \rightarrow 3b_1(\pi_4^*)$ $^1B_2$ valence transition and the (single-photon forbidden) $1a_2 \rightarrow 3sa_1\ ^1A_2$ Rydberg transition have adiabatic excitation energies below 6 eV. Multiphoton excitation studies [61] have tentatively identified the latter state at ~5.91 eV. According to the theoretical work of Gromov et al. [2], strong non-adiabatic effects can be expected above ~5.9 eV due to conical intersections between the potential energy surfaces associated with several of the low-lying states. Thus, above this energy the nuclear dynamics do not proceed on an individual surface, and therefore the structure observed between 5.9 and 6.4 eV cannot be assigned strictly to a single electronic state. Gromov et al. [2] ascribe the two lowest energy peaks, occurring at 5.669 and 5.783 eV in C_4H_4O, to excitation of non-totally symmetric vibrational modes in the $3sa_1\ ^1A_2$ Rydberg state which acquire their intensity through vibronic coupling to the $^1B_2$ valence state. Isotopic substitution has little effect on this low energy structure.

Our calculations show that the $^1A_1$ state arising from the $1a_2(\pi_3) \rightarrow 2a_2(\pi_5^*)$ transition interacts with Rydberg states. Consequently, two close-lying states are formed, with each having a strong $1a_2 \rightarrow 2a_2$ valence character and a smaller $1a_2 \rightarrow 4fa_2$ Rydberg character (Table S4). The ADC(3) vertical excitation energies of these two transitions are 7.88 and 8.08 eV, and both possess a high oscillator strength (Table 1). Another state of mixed valence-Rydberg character is predicted at slightly higher energy (8.86 eV).

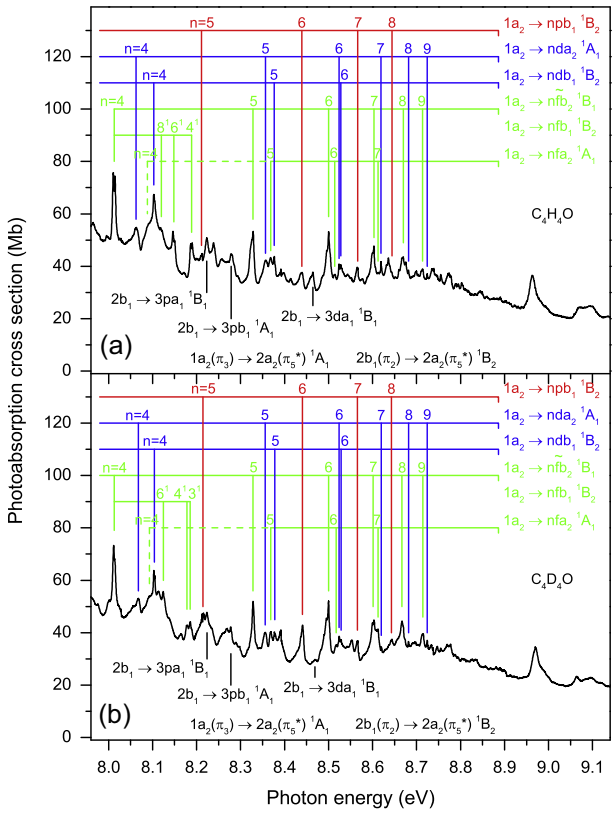

Fig. 5. The photoabsorption spectra of C_4H_4O (a) and C_4D_4O (b) showing structure due to the $1a_2(\pi_3) \rightarrow 2a_2(\pi_5^*)\ ^1A_1$ and $2b_1(\pi_2) \rightarrow 2a_2(\pi_5^*)\ ^1B_2$ valence transitions, and to various Rydberg transitions belonging to series converging onto either the $\tilde{X}\ ^2A_2$ or the $\tilde{A}\ ^2B_1$ state limit. Excitation energies and assignments are given in Tables 3 and 4.

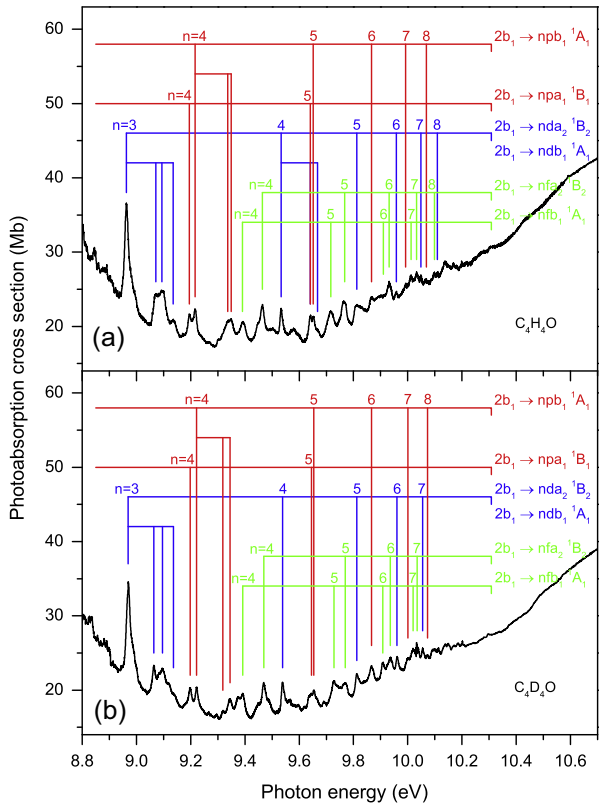

Fig. 6. The photoabsorption spectra of C_4H_4O (a) and C_4D_4O (b) showing structure due to various Rydberg transitions belonging to series converging onto the $\tilde{A}\ ^2B_1$ state limit. Excitation energies and assignments are given in Tables 5 and 6.

In this state, of B_2 symmetry, the $2b_1 \rightarrow 2a_2$ and $1a_2 \rightarrow 3b_1$ valence transitions are mixed in approximately equal proportions, and there are also contributions from various Rydberg configurations. Overall, these three states of high oscillator strength and mixed valence-Rydberg character provide a satisfactory explanation for the general shape of the photoabsorption spectrum between ~7.5 and 9.0 eV (Fig. 2).

At higher energy, the EOM-CCSD calculations predict a valence-Rydberg type state involving excitation from the $9a_1$ orbital (Table S4).

5.3. Rydberg states

5.3.1. $1a_2 \rightarrow np$ transitions

It is now generally agreed that one extended series and one series consisting of only a few members should be assigned to $1a_2 \rightarrow np$ transitions in the single-photon absorption spectrum of C_4H_4O (see Wan et al. [30] for a review of earlier assignments). The adiabatic transition into the lowest-lying of these np states gives rise to the band at 6.4740 eV which dominates the near-threshold absorption spectrum (Fig. 3). In the multiphoton absorption study performed by Ridley et al. [18], one extended p-type series was observed and assigned to the single-photon forbidden $1a_2 \rightarrow npa_1\ ^1A_2$ transitions. In addition, the $n = 3$ members of the $npb_1\ ^1B_2$ and $npb_2\ ^1B_1$ series were identified [18], thereby clarifying some previous REMPI results [62].

Our EOM-CCSD calculations give adiabatic excitation energies of 6.53, 6.67 and 6.78 eV for the $1a_2 \rightarrow 3pb_2\ ^1B_1$, $1a_2 \rightarrow 3pa_1\ ^1A_2$ and $1a_2 \rightarrow 3pb_1\ ^1B_2$ transitions, respectively, and the ADC(3) calculations give similar values (Table 1). These theoretical results are in excellent agreement with the present experimental values of 6.4740 and 6.7535 eV for the $1a_2 \rightarrow 3pb_2\ ^1B_1$ and $1a_2 \rightarrow 3pb_1\ ^1B_2$ transitions, respectively (Table 2), and that of 6.5981 eV for the forbidden $1a_2 \rightarrow 3pa_1\ ^1A_2$ transition [18]. A high oscillator strength is predicted by our calculations only for the $n = 3$ member of the $1a_2 \rightarrow npb_2\ ^1B_1$ series, with those of the higher members being much smaller (Table 1). In contrast, the calculated oscillator strengths for the $n = 4$, 5 members of the $1a_2 \rightarrow npb_1\ ^1B_2$ series are

Table 2
Energies and proposed assignments for structure associated with the $1a_2 \rightarrow 3pb_2\ ^1B_1$ and $1a_2 \rightarrow 3pb_1\ ^1B_2$ transitions in the photoabsorption spectra of C_4H_4O and C_4D_4O.

C_4H_4O			C_4D_4O		
Energy (eV)	$1a_2 \rightarrow 3pb_2\ ^1B_1$	$1a_2 \rightarrow 3pb_1\ ^1B_2$	Energy (eV)	$1a_2 \rightarrow 3pb_2\ ^1B_1$	$1a_2 \rightarrow 3pb_1\ ^1B_2$
6.4740	0^0		6.4784	0^0	
6.5333	11^1		6.5287	11^1	
6.5809	8^1		6.5896	6^1	
6.6084	6^1		6.6438	4^1	
6.6494	4^1		6.6499	3^1	
6.6902	8^2		6.7016	6^2	
6.7006	8^19^1		6.7392	4^112^1	
6.7139	6^18^1		6.7522		0^0
6.7535		0^0	6.7622	3^16^1	
6.7827	4^16^1		6.8151	3^14^1	
6.8221	4^2		6.8455		8^1
6.8462	6^28^1	13^1	6.8652		6^1
6.8596		8^1	6.9077		17^1
6.8744	6^3		6.9178		4^1
6.8904		6^1	6.9262		3^1
6.9303		4^1	6.9800		6^2
6.9799		8^19^1	7.0182		6^117^1
6.9958		6^18^1	7.0369		3^16^1
7.0271		6^2	7.0813		6^27^1
7.0646		4^16^1	7.0940		3^14^1
7.1084		4^2	7.1293		3^17^2
			7.1500		3^16^2

Table 3
Energies, proposed assignments and quantum defects for Rydberg states due to excitation from the $1a_2$ orbital in C_4H_4O.

Assignment	Energy (eV)[a]	Quantum defect (δ)	Assignment	Energy (eV)[a]	Quantum defect (δ)
$1a_2 \rightarrow npb_2\ ^1B_1$			$1a_2 \rightarrow ndb_1\ ^1B_2$		
$n = 3$	6.4740	0.625	$n = 3\ 0^0$	7.5253	−0.162
			8^1	7.6321	
$n = 4$	7.7005	0.613	6^1	7.6607	
			4^1	7.7005	
$1a_2 \rightarrow npb_1\ ^1B_2$					
			$n = 4$	8.1030	−0.167
$n = 3$	6.7535	0.474			
			$n = 5$	8.3765	−0.166
$n = 4$	7.7885	0.480			
			$n = 6$	8.5278	−0.160
$n = 5$	8.2114	0.510			
			$1a_2 \rightarrow n\tilde{f}b_2\ ^1B_1$		
			$1a_2 \rightarrow nfb_1\ ^1B_2$		
$n = 6$	8.4396	0.482			
			$n = 4\ 0^0$	8.0127	0.054
$n = 7$	8.5665	0.478	8^1	8.1200	
			6^1	8.1484	
$n = 8$	8.6443	0.503	4^1	8.1884	
$1a_2 \rightarrow ndb_2\ ^1B_1$			$n = 5$	8.3285	0.062
$n = 3\ 0^0$	7.5142	−0.149	$n = 6$	8.5002	0.065
8^1	7.6211				
6^1	7.6498		$n = 7$	8.6030	0.071
4^1	7.6889				
			$n = 8$	8.6697	0.076
$1a_2 \rightarrow nda_2\ ^1A_1$					
			$n = 9$	8.7136	0.127
$n = 4$	8.0625	−0.064			
			$1a_2 \rightarrow nfa_2\ ^1A_1$		
$n = 5$	8.3568	−0.069			
			$n = 4$	8.0880	−0.128
$n = 6$	8.5239	−0.126			
			$n = 5$	8.3684	−0.125
$n = 7$	8.6191	−0.135			
			$n = 6$	8.5137	−0.042
$n = 8$	8.6816	−0.151			
			$n = 7$	8.6128	−0.052
$n = 9$	8.7243	−0.162			

[a] Unless otherwise specified, the energy corresponds to the adiabatic transition.

Table 4
Energies, proposed assignments and quantum defects for Rydberg states due to excitation from the $1a_2$ orbital in C_4D_4O.

Assignment	Energy (eV)[a]	Quantum defect (δ)	Assignment	Energy (eV)[a]	Quantum defect (δ)
$1a_2 \rightarrow npb_2\ ^1B_1$			$1a_2 \rightarrow ndb_1\ ^1B_2$		
$n = 3$	6.4784	0.623	$n = 3\ 0^0$	7.5266	−0.163
			6^1	7.6390	
$n = 4$	7.7012	0.612	4^1	7.6942	
			3^1	7.7012	
$1a_2 \rightarrow npb_1\ ^1B_2$					
			$n = 4$	8.1041	−0.170
$n = 3$	6.7522	0.475			
			$n = 5$	8.3780	−0.173
$n = 4$	7.7881	0.480			
			$n = 6$	8.5285	−0.166
$n = 5$	8.2143	0.501			
			$1a_2 \rightarrow n\tilde{f}b_2\ ^1B_1$		
			$1a_2 \rightarrow nfb_1\ ^1B_2$		
$n = 6$	8.441	0.474			
			$n = 4\ 0^0$	8.0127	0.054
$n = 7$	8.566	0.486	6^1	8.1243	
			4^1	8.1780	
$n = 8$	8.6430	0.524	3^1	8.1857	
$1a_2 \rightarrow ndb_2\ ^1B_1$			$n = 5$	8.3285	0.062
$n = 3\ 0^0$	7.5150	−0.150	$n = 6$	8.4999	0.067
6^1	7.6267				
4^1	7.6794		$n = 7$	8.6015	0.089
$1a_2 \rightarrow nda_2\ ^1A_1$			$n = 8$	8.6670	0.125
$n = 4$	8.0675	−0.076	$n = 9$	8.7140	0.116
$n = 5$	8.3557	−0.063	$1a_2 \rightarrow nfa_2\ ^1A_1$		
$n = 6$	8.5240	−0.127	$n = 4$	8.0926	−0.140
$n = 7$	8.6199	−0.145	$n = 5$	8.3684	−0.125
$n = 8$	8.6818	−0.155	$n = 6$	8.5176	−0.074
$n = 9$	8.7244	−0.164	$n = 7$	8.6124	−0.047

[a] Unless otherwise specified, the energy corresponds to the adiabatic transition.

Table 5
Energies, proposed assignments and quantum defects for Rydberg states due to excitation from the $2b_1$ or the $7a_1$ orbital in C_4H_4O.

Assignment	Energy (eV)[a]	Quantum defect (δ)	Assignment	Energy (eV)[a]	Quantum defect (δ)
$2b_1 \rightarrow nsa_2\ ^1B_1$			$2b_1 \rightarrow nfb_1\ ^1A_1$		
$n = 3$	7.3778	0.845	$n = 4$	9.3908	0.149
$2b_1 \rightarrow npa_1\ ^1B_1$			$n = 5$	9.7167	0.203
$n = 3$	8.2230	0.446	$n = 6$	9.9100	0.153
$n = 4$	9.9154	0.503	$n = 7$	10.0124	0.216
$n = 5$	9.6414	0.482	$2b_1 \rightarrow nfa_2\ ^1B_2$		
$2b_1 \rightarrow npb_1\ ^1A_1$			$n = 4$	9.4644	−0.016
$n = 3$	8.2789	0.411	$n = 5$	9.7672	−0.016
$n = 4$	9.2159	0.470	$n = 6$	9.9320	−0.015
$n = 5$	9.6520	0.446	$n = 7$	10.0331	−0.035
$n = 6$	9.8668	0.447	$n = 8$	10.0987	−0.063
$n = 7$	9.9926	0.432	$7a_1 \rightarrow np$		
$n = 8$	10.0684	0.464	$n = 3$	15.045	0.596
$2b_1 \rightarrow nda_1\ ^1B_1$			$n = 4$	16.246	0.566
$n = 3$	8.4643	0.284	$n = 5$	16.676	0.665
$2b_1 \rightarrow nda_2\ ^1B_2$			$n = 6$	16.916	0.698
$2b_1 \rightarrow ndb_1\ ^1A_1$					
$n = 3$	8.9628	−0.180			
$n = 4$	9.5331	−0.190			
$n = 5$	9.8119	−0.237			
$n = 6$	9.9577	−0.232			
$n = 7$	10.0481	−0.235			
$n = 8$	10.1094	−0.277			

[a] Energy corresponds to the adiabatic transition.

higher than that for the $n = 3$ member. These predictions appear consistent with the experimental spectrum (Figs. 4 and 5) where we assign one extended series to the $1a_2 \rightarrow npb_1\ ^1B_2$ transitions (Table 3). Only one additional member, $n = 4$, of the $1a_2 \rightarrow npb_2\ ^1B_1$ is tentatively identified (Fig. 4). The $n = 4$ members of these p-type series would be expected to occur in an energy region containing intense valence transitions and it is possible that the Rydberg states are perturbed through vibronic interactions.

The vibrational structure associated with the $3pb_2\ ^1B_1$ and $3pb_1\ ^1B_2$ states in C_4H_4O was first observed and assigned by Pickett [9] in single-photon absorption studies. A subsequent re-examination of the spectra led Derrick et al. [50] to revise some of the assignments. Ridley et al. [18] reinvestigated this vibrational structure, in both C_4H_4O and C_4D_4O, in their REMPI experiments and obtained accurate vibrational energies. However, multiphoton excitation may result in peak intensities which differ substantially from those observed in single-photon excitation where the vibrational envelope should reflect the Franck–Condon factor connecting the ground and the Rydberg state. As our spectra for the C_4H_4O and C_4D_4O were recorded using single-photon excitation, we can compare the vibrational structure in the $3pb_2\ ^1B_1$ and $3pb_1\ ^1B_2$ absorption bands directly with that observed [16,50,51] and predicted [63,64] in the corresponding $C_4H_4O^+$ and $C_4D_4O^+$ $\tilde{X}\ ^2A_2$ state photoelectron bands.

A good overall description of the vibrational structure occurring in the $\tilde{X}\ ^2A_2$ state photoelectron bands of $C_4H_4O^+$ and $C_4D_4O^+$ has been obtained recently through calculated Franck–Condon factors, using a procedure which incorporates anharmonicity [64]. The simulations showed that the essential characteristics, namely the vibrational energies and peak intensities, in the $C_4H_4O^+$ $\tilde{X}\ ^2A_2$ state could be reproduced by including only four totally symmetric modes (ν_4^+, ν_5^+, ν_6^+ and ν_8^+) in the calculations. (The vibrational

Table 6
Energies, proposed assignments and quantum defects for Rydberg states due to excitation from the $2b_1$ orbital in C_4D_4O.

Assignment	Energy (eV)[a]	Quantum defect (δ)[b]	Assignment	Energy (eV)[a]	Quantum defect (δ)[b]
$2b_1 \rightarrow nsa_1\ ^1B_1$			$2b_1 \rightarrow nda_2\ ^1B_2$, $2b_1 \rightarrow ndb_1\ ^1A_1$		
$n = 3$	7.3904	0.843	$n = 3$	8.9697	−0.180
$2b_1 \rightarrow npa_1\ ^1B_1$			$n = 4$	9.5385	−0.186
$n = 3$	8.2235	0.450	$n = 5$	9.8124	−0.203
$n = 4$	9.1984	0.509	$n = 6$	9.9607	−0.197
$n = 5$	9.6448	0.494	$n = 7$	10.0548	−0.231
$2b_1 \rightarrow npb_1\ ^1A_1$			$2b_1 \rightarrow nfb_1\ ^1A_1$		
$n = 3$	8.2778	0.416	$n = 4$	9.3916	0.162
$n = 4$	9.2218	0.472	$n = 5$	9.7286	0.183
$n = 5$	9.6542	0.462	$n = 6$	9.9083	0.216
$n = 6$	9.8664	0.493	$n = 7$	10.0195	0.215
$n = 7$	10.0010	0.417	$2b_1 \rightarrow nfa_2\ ^1B_2$		
$n = 8$	10.0726	0.508	$n = 4$	9.4692	−0.011
$2b_1 \rightarrow nda_1\ ^1B_1$			$n = 5$	9.7697	−0.005
$n = 3$	8.4688	0.285	$n = 6$	9.9362	0.007
			$n = 7$	10.0346	0.034

[a] Energy corresponds to the adiabatic transition.
[b] Quantum defect derived through use of an estimated $\tilde{A}\ ^2B_1$ state adiabatic ionisation energy of 10.315 eV.

modes are numbered as recommended by Herzberg [65].) The corresponding band in $C_4D_4O^+$ was satisfactorily reproduced in simulations incorporating the ν_3^+, ν_4^+, ν_5^+ and ν_6^+ modes. However, some weak features appearing in the experimental spectrum [51] remain unaccounted for in this interpretation where only progressions involving the totally symmetric vibrational modes are considered. Trofimov et al. [63] have shown that these features are the result of vibronic coupling between the $\tilde{X}\ ^2A_2$ and the $\tilde{A}\ ^2B_1$ states, induced by non-totally symmetric b_2 vibrational modes. Interestingly, some peaks in the ZEKE spectrum of C_4H_4O [52] were interpreted as being due not only to modes of b_2 symmetry, but also of a_2 or b_1 symmetry.

Table 2 provides a summary of our assignments of the vibrational progressions associated with the $3pb_2\ ^1B_1$ and $3pb_1\ ^1B_2$ states in C_4H_4O and C_4D_4O (Fig. 3). Deuteration modifies the structure, and in both isotopomers the vibrational envelope observed in absorption strongly resembles that in the corresponding photoelectron band [16,51]. In C_4H_4O, the absorption bands are dominated by excitations involving the ν_8, ν_6 and ν_4 modes, either alone or in combination with each other. We obtain energies of 106.9, 134.4 and 175.4 meV for the ν_8, ν_6 and ν_4 modes, respectively, in the $3pb_2\ ^1B_1$ state, in good agreement with the values reported by Ridley et al. [18]. An additional totally symmetric mode, namely ν_3 with an energy of 183.0 meV, was observed by Ridley et al. [18], and also by Philis [66] in a REMPI study of the 3d Rydberg states. It is conceivable that this mode is responsible for the high energy shoulder we observe on the peak at 6.6494 eV (Fig. 3).

Although most of the absorption bands can be assigned to excitations involving only totally symmetric vibrational modes, our analysis suggests that some of the structure should be ascribed to non-totally symmetric modes. In the $3pb_2\ ^1B_1$ state in C_4H_4O, we tentatively assign a peak to excitation of the ν_{11} (a_2) mode, and another to excitation of the ν_9 (a_2) mode in combination with a single quantum of the ν_8 (a_1) mode. In the $3pb_1\ ^1B_2$ state, two bands are tentatively associated with the ν_9 (a_2) and ν_{13} (b_1) modes.

In the corresponding states of C_4D_4O, the vibrational progressions are mainly associated with the ν_6, ν_4 and ν_3 modes (Table 2) for which we obtain energies of 111.2, 165.4 and 171.5 meV, respectively, in the $3pb_2\ ^1B_1$ state. In addition, we tentatively assign structure in the $3pb_2\ ^1B_1$ and in the $3pb_1\ ^1B_2$ state to excitations involving the ν_{11} (a_2) or ν_{12} (b_1) modes, or to the ν_{17} (b_2) mode, respectively.

5.3.2. $1a_2 \rightarrow nd$ transitions

According to our calculations (Table 1), for a given principal quantum number, the ordering of the single-photon allowed $1a_2 \rightarrow nd$ excitations is $ndb_2\ ^1B_1$, $nda_2\ ^1A_1$, $ndb_1\ ^1B_2$, in order of increasing energy. The transition energies of the two forbidden nda_1 and $n\tilde{d}a_1\ ^1A_2$ excitations are predicted to lie on either side of, and close to, that for the $ndb_2\ ^1B_1$ transition. For $n > 3$, the oscillator strengths of the $nda_2\ ^1A_1$ and $ndb_1\ ^1B_2$ states are calculated to be considerably higher than that for the $ndb_2\ ^1B_1$ state. These predictions are consistent with those obtained previously [29,30,32] but the availability of both the adiabatic and the vertical transition energies in the present calculations facilitates the absorption band assignments.

Ridley et al. [17,18] observed two extended d-type Rydberg series and, by taking into account multiphoton excitation propensity rules and the polarisation dependence of the signal, have ascribed A_1 symmetry to one of the series, and non-A_1 symmetry to the other. The latter series is most likely to be one of the $nda_1\ ^1A_2$ series [18]. For $n > 5$, the quantum defects of these series are fairly regular, with the transition energy of the $^1A_1$ state being higher than that of the $^1A_2$ state.

Philis [66] has also used the REMPI technique to study the 3d Rydberg states and their associated vibrational structure. The results were interpreted as showing that the excitation energies of the five states were $A_2(1) \approx A_2(2) < A_1 < B_1 < B_2$ in order of increasing energy. The transition energies for the $3da_2\ ^1A_1$, $3db_2\ ^1B_1$ and $3db_1\ ^1B_2$ states were in accord with those measured by Ridley et al. This sequence is only partially consistent with the present calculations which predict that the excitation energy of the $nda_2\ ^1A_1$ state is always greater than that of the $ndb_2\ ^1B_1$ state.

Two extended series attributed to $1a_2 \rightarrow nd$ transitions appear in our photoabsorption spectrum (Figs. 4 and 5, and Table 3). One of these series ($1a_2 \rightarrow nda_2\ ^1A_1$) clearly corresponds to that observed by Ridley et al., although the $n = 3$ state (at 7.4251 eV [18]) does not give rise to a discernible peak in the single-photon absorption spectrum. The second extended series is assigned to the $1a_2 \rightarrow ndb_1\ ^1B_2$ transitions, with the $n = 3$ member occurring at 7.5253 eV (in excellent agreement with the calculated adiabatic energy of 7.54 eV (Table 1)). The band observed at 7.5142 eV is assigned to the $3db_2\ ^1B_1$ state. It is noticeable that the bands associated with the $3db_2\ ^1B_1$ and the $3db_1\ ^1B_2$ states, and this is also the case for some f-type Rydberg states, exhibit a doublet profile. Such profiles were not observed in previous single-photon absorption studies performed at poorer optical resolution or in the REMPI experiments employing cooled molecular beams. For the 3d states, the separation between the peaks in the doublet is ~2 meV. The cause of the doublet profile is not understood at present. For an absorption band displaying a doublet profile, the excitation energy given in Table 3 represents the midpoint.

The extended series observed for the $1a_2 \rightarrow nda_2\ ^1A_1$ and the $1a_2 \rightarrow ndb_1\ ^1B_2$ transitions, and the appearance of only the $n = 3$ member of the $1a_2 \rightarrow ndb_2\ ^1B_2$ series, are consistent with the high oscillator strengths calculated for the first two series and the low oscillator strength predicted for the $1a_2 \rightarrow ndb_2\ ^1B_1$ series.

Vibrational structure associated with the $3db_2\ ^1B_1$ and $3db_1\ ^1B_2$ states can be assigned to excitations involving the ν_4, ν_6 and ν_8 modes in C_4H_4O (Fig. 4 and Table 3), and to the ν_3, ν_4 and ν_6 modes in C_4D_4O (Fig. 4 and Table 4).

5.3.3. $1a_2 \rightarrow nf$ transitions

The important role played by transitions into f-type Rydberg states in furan was first identified in REMPI experiments [18]

where one long series of A_2 symmetry and several shorter series of non-A_2 symmetry were observed. Prior to that study, excitations due to $1a_2 \rightarrow nf$ transitions had not been assigned as such in the single-photon absorption spectra. However, a repeated analysis of these spectra resulted in some of the bands previously associated with d-type states being reassigned to f-type states [18]. Our theoretical results (Table 3) indicate that there are several $1a_2 \rightarrow 4f$, 5f transitions possessing sufficient oscillator strength to give rise to observable absorption bands.

In our spectrum of C_4H_4O (Fig. 5), one strong f-type Rydberg series, whose $n = 4$ member occurs at 8.0127 eV, is discernible up to $n = 9$. A similar series was observed by Ridley et al. [18] and classified as having non-A_2 symmetry. Guided by our calculations, we assign this series to the $1a_2 \rightarrow n\tilde{f}b_2\ ^1B_1$ and $1a_2 \rightarrow nfb_1\ ^1B_2$ transitions, whose theoretical vertical excitation energies are almost identical (Table 1). The $n = 4$ member of this series exhibits vibrational structure (Table 3).

We tentatively associate the shoulder at 8.0880 eV with the perturbed $4fa_2\ ^1A_1$ state. The interaction between this Rydberg state and the neighbouring $^1A_1$ valence state, due to the $1a_2 \rightarrow 2a_2$ transition (Table S4), results in a high predicted oscillator strength ($f = 0.120$) and a slightly shifted excitation energy for this mixed Rydberg-valence state (Table 1). The observed energy separation between the band ascribed to the $4\tilde{f}b_2\ ^1B_1/4fb_1\ ^1B_2$ state and that due to the $4fa_2\ ^1A_1$ state is ~0.08 eV, which is in reasonable agreement with the difference between the corresponding calculated (ADC(3)) energies of 7.98 and 8.08 eV (Table 1). Our calculations give a vertical excitation energy of 8.34 eV and an oscillator strength of $f = 0.012$ for the $1a_2 \rightarrow 5fa_2\ ^1A_1$ transition. We tentatively associate this transition with the band observed at 8.3684 eV. It seems likely that the series we have attributed to the $1a_2 \rightarrow nfa_2\ ^1A_1$ transitions is the same as the unassigned, non-A_2 symmetry, series reported by Ridley et al. [18].

Several absorption bands remain unidentified in the energy range between ~8.2 and 8.4 eV (Fig. 5). As these bands appear at approximately the same excitation energies in the spectra of C_4H_4O as they do in the spectra of C_4D_4O, they are probably due to adiabatic transitions into Rydberg states. The $1a_2 \rightarrow 5fb_2\ ^1B_1$ and the $1a_2 \rightarrow 5\tilde{f}b_1\ ^1B_2$ transitions are predicted to occur in this region (Table 1), but associating these excitations with specific absorption bands is difficult. Our theoretical results suggest that the short series of A_2 symmetry observed by Ridley et al. [18] should be attributed to the $1a_2 \rightarrow n\tilde{f}a_1\ ^1A_2$ transitions.

5.3.4. $1a_2 \rightarrow ns$ transitions

Although bands due to the $1a_2 \rightarrow ns$ transitions do not appear in the present single-photon absorption spectrum, s-type Rydberg states have been observed in multiphoton absorption studies [61,62]. The experimental excitation energies of 5.91, 7.52 and 8.10 eV for the $n = 3$, 4, 5 members, respectively, are in good agreement with our calculated values (Table 1).

5.4. Transitions from the $2b_1$ orbital

In previous assignments of the absorption bands due to excitation from the $2b_1$ orbital [15,30,50], the main series was attributed to the $2b_1 \rightarrow nsa_1\ ^1B_1$ transitions, with the first member ($n = 3$) being assigned to the prominent band observed at 7.3778 eV (Fig. 4). In addition, some weaker bands were ascribed to various *n*p or *n*d series. The present theoretical results suggest a major revision to these earlier assignments wherein the main series is associated with d-type Rydberg states and weaker series to *n*p and *n*f excitations. Transitions into f-type states have not been considered previously. Our analysis suggests that absorption bands due to the *n*s series are observed only for the $n = 3$, and possibly the $n = 4$, members.

Fig. 6 shows the photoabsorption spectra of C_4H_4O and C_4D_4O in the energy range 8.9–10.4 eV. In accord with previous interpretations, the $2b_1 \rightarrow 3sa_1\ ^1B_1$ transition is associated with the band observed at 7.3778 eV in C_4H_4O. The calculated vertical excitation energy (7.54 eV (Table 1)) and high oscillator strength ($f = 0.024$) are consistent with the experimental results. However, the $n = 4$ member of this series is predicted to have a vertical excitation energy of 9.11 eV and a low oscillator strength ($f = 0.002$). At about the same energy, the calculations predict the $2b_1 \rightarrow 3da_2\ ^1B_2$ (at 9.09 eV and with $f = 0.053$) and the $2b_1 \rightarrow 3db_1\ ^1A_1$ (at 9.10 eV with $f = 0.040$) transitions. Thus, we reassign the peak observed at 8.9628 eV to the $n = 3$ members of the $2b_1 \rightarrow nda_2\ ^1B_2$ and the $2b_1 \rightarrow ndb_1\ ^1A_1$ series. The absorption bands associated with higher members of these series now include some of the structure previously attributed to the ns series. The shoulder on the high energy side of the peak at 8.9628 eV may be due to the $2b_1 \rightarrow 4sa_1\ ^1B_1$ transition. The transition energies and assignments of Rydberg states due to excitations from the $2b_1$ orbital are given in Tables 5 and 6 for C_4H_4O and C_4D_4O, respectively.

According to our theoretical results, both single-photon allowed p-series, namely $2b_1 \rightarrow npa_1\ ^1B_1$ and $2b_1 \rightarrow npb_1\ ^1A_1$, possess reasonable oscillator strengths. In the experimental spectrum (Fig. 6) one extended p-series ($\delta = 0.47$) is observed whose $n = 4$ member occurs at 9.2159 eV. We tentatively assign this series to the $2b_1 \rightarrow npb_1\ ^1A_1$ transitions, for which the calculated excitation energy of the $n = 4$ member is 9.33 eV. If we assume that the quantum defect of the $n = 3$ member is similar to those of the higher members, then the resulting estimated excitation energy is 8.18 eV. Thus, we attribute the peak appearing at 8.2789 eV to the $2b_1 \rightarrow 3pb_1\ ^1A_1$ transition (whose calculated excitation energy and oscillator strength are 8.28 eV and $f = 0.021$, respectively (Table 1)).

The peak at 9.1954 eV might be associated with the $n = 4$ member of the second p-type series ($2b_1 \rightarrow npa_1\ ^1B_1$), although an alternative assignment of this peak is to vibrational structure associated with the $3da_2\ ^1B_2$ and $3db_1\ ^1A_1$ states. If we assume the former assignment, then the peak at 9.6614 eV might be associated with the next ($n = 5$) member. The first member of this series has a calculated vertical excitation energy of 8.20 eV and an oscillator strength of 0.005, and is tentatively assigned to the peak observed at 8.2230 eV.

Another series can be identified in the experimental spectrum whose first member appears at 9.4644 eV, leading to a quantum defect $\delta = -0.02$, for $n = 4$. There is no evidence of a lower member belonging to this series, thereby suggesting an assignment to an f-type series. The theoretical vertical excitation energies of the $2b_1 \rightarrow 4fb_1\ ^1A_1$, $2b_1 \rightarrow 4\tilde{f}b_1\ ^1A_1$ and $2b_1 \rightarrow 4fa_2\ ^1B_2$ transitions are 9.57, 9.59 and 9.60 eV, respectively (Table 1), with the latter transition having the highest oscillator strength. Thus, this series is tentatively assigned to the $2b_1 \rightarrow nfa_2\ ^1B_2$ transitions, although it is conceivable that more than one of these series contributes to the observed bands. There is also some evidence of a second f-type series in the experimental spectrum. The second series is tentatively assigned to the $2b_1 \rightarrow nfb_1\ ^1A_1$transitions although the measured quantum defect (Table 5) is higher than predicted (Table S3).

Several of the Rydberg states associated with excitations originating from the $2b_1$ orbital display vibrational structure (Fig. 6). This structure cannot be assigned in a simple manner [63].

5.5. Transitions from the $7a_1$ orbital

The present spectrum (Fig. 7) confirms the Rydberg series, due to excitation from the $7a_1$ orbital, reported by Rennie et al. [16].

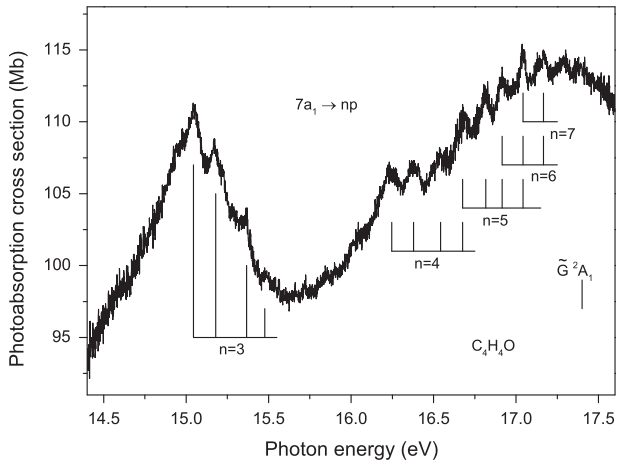

Fig. 7. The photoabsorption spectrum of C_4H_4O showing structure associated with the $7a_1 \rightarrow np$ series converging onto the $\tilde{G}\,^2A_1$ state limit. Excitation energies and assignments are given in Table 6.

The derived quantum defect, of ~0.6 (Table 5), suggests that the absorption bands should be associated with one, or more, of the three allowed p-series. The vibrational spacing of ~133 meV suggests excitation of the ν_6 mode. It appears that this series is analogous to the $npe_{1u}\,^1E_{1u}$ series, with δ~0.47 [67], converging onto the $\tilde{F}\,^1A_{1g}$ state limit in benzene.

6. Summary

The photoabsorption spectra of C_4H_4O and C_4D_4O have been measured between 5.5 and 17.7 eV using the FTS attached to the Soleil synchrotron radiation source. The highly resolved spectra display several broad bands due to transitions into valence states and some much narrower structure ascribed to Rydberg series. Vertical excitation energies and oscillator strengths have been computed using the ADC(2), ADC(3) and EOM-CCSD approaches, in conjunction with extended basis sets, yielding a consistent description of the valence and Rydberg states. The basis sets employed in these calculations have included f-type Rydberg functions. This has proved to be an important development because several of the Rydberg series appearing in the experimental spectrum arise from transitions into f-type states. Adiabatic transition energies have been estimated.

Guided by the theoretical results, a reasonable interpretation has been obtained for the low-lying valence bands due to $\pi \rightarrow \pi^*$ excitations as well as for the principal Rydberg series converging onto the $\tilde{X}\,^2A_2$ or the $\tilde{A}\,^2B_1$ state limits. For the lowest ionisation threshold, two p-type, two d-type and two f-type Rydberg series have been identified and assigned in the present single-photon absorption spectrum. In addition, several single-photon forbidden series of A_2 symmetry, observed in multiphoton absorption studies [17,18,61,62], have been assigned. Our results show that f-type Rydberg states make a significant contribution to the single-photon absorption spectrum of furan, contrary to earlier interpretations. Our theoretical predictions have led to a substantial revision to the assignments of the Rydberg series converging onto the $\tilde{A}\,^2B_1$ state limit. The prominent Rydberg series previously assigned to the $2b_1 \rightarrow nsa_1\,^1B_1$ transitions, has been shown, based upon calculated excitation energies and oscillator strengths, to arise from the $2b_1 \rightarrow nda_2\,^1B_2$ and $2b_1 \rightarrow ndb_1\,^1A_1$ transitions. One p-type and one (or possibly more) f-type Rydberg series converging onto the $\tilde{A}\,^2B_1$ state limit have also been observed. f-type Rydberg series associated with this limit have not been reported previously. Finally, a Rydberg series converging onto the $(7a_1)^{-1}$ $\tilde{G}\,^2A_1$ state limit has been observed.

Several of the absorption bands associated with Rydberg states display vibrational structure which resembles that in the corresponding photoelectron band. The overlapping vibrational progressions associated with the $1a_2 \rightarrow 3pb_2\,^1B_1$ and $1a_2 \rightarrow 3pb_1\,^1B_2$ transitions have been re-examined, in both C_4H_4O and C_4D_4O, and new assignments have been proposed for some of the absorption bands. It appears that part of the structure is due to excitation of non-totally symmetric vibrational modes.

The Rydberg series due to excitation from the $2b_1$ orbital in furan exhibit considerably more structure than do the corresponding series in pyrrole [68] or thiophene [47,69].

Further theoretical studies are required to obtain an improved description of the increase in photoabsorption cross section at energies above ~10 eV. Such rises in cross section are commonly observed in five- or six-membered ring-type molecules [70,71] and are generally attributed to transitions into many, closely spaced, valence states.

Acknowledgments

The authors are grateful to the technical staff of the Soleil synchrotron radiation facility for their efficient operation of the storage ring. ABT gratefully acknowledges Grant No. 4.1504.2014/K from the Ministry of Education and Science of the Russian Federation. DMPH thanks Stephen Pratt (Argonne National Laboratory) for useful discussions concerning the nodal properties of the furan molecular orbitals. The authors thank the Referee for helpful comments and suggestions regarding the vibrational assignments shown in Fig. 3.

Appendix A. Supplementary material

Supplementary data associated with this article can be found, in the online version, at http://dx.doi.org/10.1016/j.jms.2015.03.002.

References

[1] E.V. Gromov, A.B. Trofimov, N.M. Vitkovskaya, J. Schirmer, H. Köppel, J. Chem. Phys. 119 (2003) 737.
[2] E.V. Gromov, A.B. Trofimov, N.M. Vitkovskaya, H. Köppel, J. Schirmer, H.-D. Meyer, L.S. Cederbaum, J. Chem. Phys. 121 (2004) 4585.
[3] E.V. Gromov, V.S. Reddy, F. Gatti, H. Köppel, J. Chem. Phys. 139 (2013) 234306.
[4] N. Gavrilov, S. Salzmann, C.M. Marian, Chem. Phys. 349 (2008) 269.
[5] E.V. Gromov, A.B. Trofimov, F. Gatti, H. Köppel, J. Chem. Phys. 133 (2010) 164309.
[6] T. Fuji, Y.-I. Suzuki, T. Horio, T. Suzuki, R. Mitrić, U. Werner, V. Bonačič-Koutecký, J. Chem. Phys. 133 (2010) 234303.
[7] M. Stenrup, Å. Larson, Chem. Phys. 379 (2011) 6.
[8] E.V. Gromov, C. Lévêque, F. Gatti, I. Burghardt, H. Köppel, J. Chem. Phys. 135 (2011) 164305.
[9] L.W. Pickett, J. Chem. Phys. 8 (1940) 293.
[10] W.C. Price, A.D. Walsh, Proc. Roy. Soc. A179 (1941) 201.
[11] L.W. Pickett, N.J. Noeflich, T.-C. Liu, J. Am. Chem. Soc. 73 (1951) 4865.
[12] K. Watanabe, T. Nakayama, J. Chem. Phys. 29 (1958) 48.
[13] B. Nordén, R. Håkansson, P.B. Pederson, E.W. Thulstrup, Chem. Phys. 33 (1978) 355.
[14] L. Nyulaszi, T. Veszpremi, Acta Chim. Hung. 130 (1993) 811.
[15] M.H. Palmer, I.C. Walker, C.C. Ballard, M.F. Guest, Chem. Phys. 192 (1995) 111.
[16] E.E. Rennie, C.A.F. Johnson, J.E. Parker, D.M.P. Holland, D.A. Shaw, M.A. MacDonald, M.A. Hayes, L.G. Shpinkova, Chem. Phys. 236 (1998) 365.
[17] T. Ridley, K.P. Lawley, M.H.S.N. Al-Kahali, R.J. Donovan, Chem. Phys. Lett. 390 (2004) 376.
[18] T. Ridley, K.P. Lawley, R.J. Donovan, Phys. Chem. Chem. Phys. 6 (2004) 5304.
[19] U. Jacovella, D.M.P. Holland, S. Boyé-Péronne, D. Joyeux, L.E. Archer, N. de Oliveira, L. Nahon, R.R. Lucchese, H. Xu, S.T. Pratt, J. Chem. Phys. 141 (2014) 114303.
[20] U. Jacovella, D.M.P. Holland, S. Boyé-Péronne, B. Gans, N. de Oliveira, D. Joyeux, L.E. Archer, R.R. Lucchese, H. Xu, S.T. Pratt, J. Chem. Phys., (submitted).
[21] H. Xu, U. Jacovella, B. Ruscic, S.T. Pratt, R.R. Lucchese, J. Chem. Phys. 136 (2012) 154303.
[22] W.L. Jorgensen, L. Salem, The Organic Chemist's Book of Orbitals, Academic Press, New York, 1973.

[23] U. Fano, J.W. Cooper, Rev. Mod. Phys. 40 (1968) 441.
[24] N. de Oliveira, D. Joyeux, D. Phalippou, J.C. Rodier, F. Polack, M. Vervloet, L. Nahon, Rev. Sci. Instrum. 80 (2009) 043101.
[25] H. Nakatsuji, O. Kitao, T. Yonezawa, J. Chem. Phys. 83 (1985) 723.
[26] L. Serrano-Andrés, M. Merchán, I. Nebot-Gil, B.O. Roos, M. Fülscher, J. Am. Chem. Soc. 115 (1993) 6184.
[27] H. Nakano, T. Tsuneda, T. Hashimoto, K. Hirao, J. Chem. Phys. 104 (1996) 2312.
[28] A.B. Trofimov, J. Schirmer, Chem. Phys. 224 (1997) 175.
[29] O. Christiansen, P. Jørgensen, J. Am. Chem. Soc. 120 (1998) 3423.
[30] J. Wan, J. Meller, M. Hada, M. Ehara, H. Nakatsuji, J. Chem. Phys. 113 (2000) 7853.
[31] R. Burcl, R.D. Amos, N.C. Handy, Chem. Phys. Lett. 355 (2002) 8.
[32] M. Pastore, C. Angeli, R. Cimiraglia, Chem. Phys. Lett. 426 (2006) 445.
[33] X. Li, J. Paldus, J. Phys. Chem. A 114 (2010) 8591.
[34] A.B. Trofimov, G. Stelter, J. Schirmer, J. Chem. Phys. 111 (1999) 9982.
[35] A.B. Trofimov, G. Stelter, J. Schirmer, J. Chem. Phys. 117 (2002) 6402.
[36] P.H.P. Harbach, M. Wormit, A. Dreuw, J. Chem. Phys. 141 (2014) 064113.
[37] J. Schirmer, Phys. Rev. A 26 (1982) 2395.
[38] A.B. Trofimov, J. Schirmer, J. Phys. B 28 (1995) 2299.
[39] J.H. Starcke, M. Wormit, A. Dreuw, J. Chem. Phys. 130 (2009) 024104.
[40] G. Wälz, D. Kats, D. Usvyat, T. Korona, M. Schütz, Phys. Rev. A 86 (2012) 052519.
[41] M. Wormit, D.R. Rehn, P.H.P. Harbach, J. Wenzel, C.M. Krauter, E. Epifanovsky, A. Dreuw, Mol. Phys. 112 (2014) 774.
[42] H. Sekino, R.J. Bartlett, Int. J. Quantum Chem. Symp. 18 (1984) 255.
[43] J. Geertsen, M. Rittby, R.J. Bartlett, Chem. Phys. Lett. 164 (1989) 57.
[44] J.F. Stanton, R.J. Bartlett, J. Chem. Phys. 98 (1993) 7029.
[45] T. Korona, H.J. Werner, J. Chem. Phys. 118 (2003) 3006.
[46] L. Nahon, N. de Oliveira, G.A. Garcia, J.-F. Gil, B. Pilette, O. Marcouillé, B. Lagarde, F. Polack, J. Synchrotron Radiat. 19 (2012) 508.
[47] D.M.P. Holland, A.B. Trofimov, E.A. Seddon, E.V. Gromov, T. Korona, N. de Oliveira, L.E. Archer, D. Joyeux, L. Nahon, Phys. Chem. Chem. Phys. 16 (2014) 21629.
[48] N. de Oliveira, D. Joyeux, K. Ito, L Archer, J.-F. Gil, L. Nahon, 2015 (in preparation).
[49] See http://webbook.nist.gov/ for NIST Chemistry WebBook.
[50] P.J. Derrick, L. Åsbrink, O. Edqvist, B.-Ö. Jonsson, E. Lindholm, Int. J. Mass Spectrom. Ion Phys. 6 (1971) 161.
[51] P.J. Derrick, L. Åsbrink, O. Edqvist, E. Lindholm, Spectrochim. Acta 27A (1971) 2525.
[52] J. Yang, J. Li, Y. Mo, J. Chem. Phys. 125 (2006) 174313.
[53] Y. Shao et al., Mol. Phys. 113 (2015) 184.
[54] H.-J. Werner, P.J. Knowles, F.R. Manby, M. Schütz, P. Celani, G. Knizia, T. Korona, R. Lindh, A. Mitrushenkov, G. Rauhut, T.B. Adler, R.D. Amos, A. Bernhardsson, A. Berning, D.L. Cooper, M.J.O. Deegan, A.J. Dobbyn, F. Eckert, E. Goll, C. Hampel, A. Hesselmann, G. Hetzer, T. Hrenar, G. Jansen, C. Köppl, Y. Liu, A.W. Lloyd, R.A. Mata, A.J. May, S.J. McNicholas, W. Meyer, M.E. Mura, A. Nicklass, P. Palmieri, K. Pflüger, R. Pitzer, M. Reiher, T. Shiozaki, H. Stoll, A.J. Stone, R. Tarroni, T. Thorsteinsson, M. Wang, A. Wolf, MOLPRO, version 2012.1, A Package of Ab Initio Programs, 2012; see <http://www.molpro.net>.
[55] H.-J. Werner, P.J. Knowles, G. Knizia, F.R. Manby, M. Schütz, Comput. Mol. Sci. 2 (2012) 242.
[56] F. Mata, M.C. Martin, G.O. Sørensen, J. Mol. Struct. 48 (1978) 157.
[57] T.H. Dunning, J. Chem. Phys. 90 (1989) 1007.
[58] R.A. Kendall, T.H. Dunning, R.J. Harrison, J. Chem. Phys. 96 (1992) 6796.
[59] K. Kaufmann, W. Baumeister, M. Jungen, J. Phys. B 22 (1989) 2223.
[60] H. Köppel, W. Domcke, L.S. Cederbaum, Adv. Chem. Phys. 57 (1984) 59.
[61] J.L. Roebber, D.P. Gerrity, R. Hemley, V. Vaida, Chem. Phys. Lett. 75 (1980) 104.
[62] C.D. Cooper, A.D. Williamson, J.C. Miller, R.N. Compton, J. Chem. Phys. 73 (1980) 1527.
[63] A.B. Trofimov, H. Köppel, J. Schirmer, J. Chem. Phys. 109 (1998) 1025.
[64] S. Bonness, B. Kirtman, M. Huix, A.J. Sanchez, J.M. Luis, J. Chem. Phys. 125 (2006) 014311.
[65] G. Herzberg, Molecular Spectra and Molecular Structure, Vol. II, Infrared and Raman Spectra of Polyatomic Molecules, Van Nostrand Reinhold, New York, 1945.
[66] J.G. Philis, Spectrochim. Acta A67 (2007) 1357.
[67] E.E. Rennie, C.A.F. Johnson, J.E. Parker, D.A. Shaw, D.M.P. Holland, M.A. Hayes, Chem. Phys. 229 (1998) 107.
[68] E.E. Rennie, C.A.F. Johnson, J.E. Parker, R. Ferguson, D.M.P. Holland, D.A. Shaw, Chem. Phys. 250 (1999) 217.
[69] E.E. Rennie, D.M.P. Holland, D.A. Shaw, C.A.F. Johnson, J.E. Parker, Chem. Phys. 306 (2004) 295.
[70] M. Stener, P. Decleva, D.M.P. Holland, D.A. Shaw, J. Phys. B 44 (2011) 075203.
[71] D.M.P. Holland, D.A. Shaw, S. Coriani, M. Stener, P. Decleva, J. Phys. B 46 (2013) 175103.